UNIVERSITÀ DI PARMA
ARCHIVIO DELLA RICERCA

University of Parma Research Repository

FEM analysis of a HF coreless transformer for automotive applications

This is the peer reviewd version of the followng article:

Original
FEM analysis of a HF coreless transformer for automotive applications / Daniele, S., Spaggiari, D., Santoro, D., Cova, P., Delmonte, N.. - In: MICROELECTRONICS RELIABILITY. - ISSN 0026-2714. - 126:(2021). [10.1016/j.microrel.2021.114224]

Availability:
This version is available at: 11381/2905033 since: 2024-10-25T17:53:44Z

Publisher:
Elsevier

Published
DOI:10.1016/j.microrel.2021.114224

Terms of use:

Anyone can freely access the full text of works made available as "Open Access". Works made available

Publisher copyright

note finali coverpage

(Article begins on next page)

13 November 2026

FEM Analysis of a HF Coreless Transformer for Automotive Applications

Simone Daniele[a,b], Davide Spaggiari[a], Danilo Santoro[a], Paolo Cova[a*], Nicola Delmonte[a]
[a] Dipartimento di Ingegneria e Architettura, University of Parma, Italy
[b] Federal-Mogul Italy s.r.l., Carpi (MO), Italy

Abstract – In this research work, a high-frequency converter with GaN devices is proposed for a reliable specific automotive application. Core of the circuit is a high-frequency transformer, able to work at 5 MHz switching frequency with relevant power absorption peaks. 3D finite element method (FEM) simulations are provided for different transformers and a first prototype has been tested. Considerations about geometry, mutual inductance, current limitations, and thermal behavior are explored through dedicated simulations.

1. Introduction

Power demand and power density of the on-board devices are increased in modern power electronics. All the more so for new generation vehicles, where specific reliable boost circuits are required. Different types of loads have to be supplied using the standard bus at 12 V or 24 V. In this work, a 96 V power load requires an impulsive power absorption by a dedicated DC/DC conversion stage. In fact, the power profile changes from 0 kW to 4 kW in 50 µs, which is a relevant challenge for commonly used Power Supply Units (PSU). Moreover, this power profile burst is repeated several times per second. Reliability issues are strongly related to the electrical requirements. Automotive environment introduces space limitations, mechanical vibrations, electrical noises from other circuits, and constraints due to scalability and high-volume production.

A first solution can be a capacitor bank between the power converter and the load, capable to supply power peaks. However, this solution results in a very expensive, bulky and not reliable architecture. In fact, due to the space limitations, aluminum electrolytic capacitors should be used to obtain relevant capacitance values. For these components, lifetime in hours can be estimated through the equation:

$$L = L_b \times M_v \times 2^{((T_m - T_c)/10)} \quad (1)$$

where L_b in hours is the base life at an elevated core temperature T_m, and T_c is the core temperature, and M_v is the voltage multiplier given by

$$M_v = 4.3 - 3.3 \times (V_a/V_r) \quad (2)$$

where V_a and V_r are the applied and the rated DC voltages, respectively.

Considering the requirements of the application, the voltage multiplier term and the exponential temperature coefficient will not introduce any improvement to the estimated lifetime. According to the material and electrolytic capacitor type, the lifetime results around 20 thousand hours, which is a limit for car manufacturers. Thus, failure in time (FIT) of the capacitor bank depends also on the number of capacitors and the lifetime of the singular capacitor competes with the lifetime of the other capacitors of the bank. In fact, random failures are most likely to occur by increasing the number of capacitors, which makes necessary an appropriate series-parallel connection.

Therefore, an estimation of 10 to 100 FIT rate can be obtained [1]. Major failure mechanisms in capacitors are related to high ambient temperatures, over voltage stresses, excess of ripple currents, and continuous charge/discharge cycles. A change of the component technology could increase the circuit reliability. Using MLCC capacitors, it is possible to obtain approximately 10 to 100 times lower FIT rate than with electrolytic capacitors, resulting in a more promising solution [2]. Nevertheless, the capacitance density values are limited, resulting in huge circuits sizes.

FIT rate of inductors, also in power electronics applications, is generally 10 to 100 times smaller than the one of capacitors [3].

For an improved reliability and a size reduction of the whole circuit, an alternative solution can be developed with a high switching frequency converter. In this paper we explore the possibility to develop coreless transformers with preliminary numerical analysis and a first prototype. In Figure 1 the proposed converter architecture is shown.

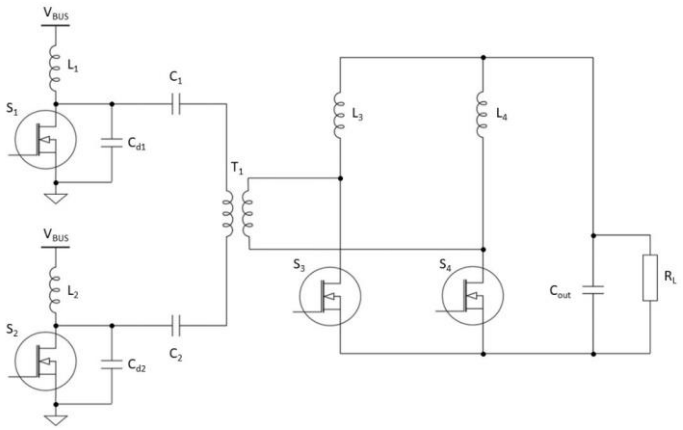

Figure 1. Architecture of the DC/DC high-frequency converter.

The converter should be properly designed for the necessary current requirements and the power peak absorptions. The galvanic isolation required by the automotive application is provided by the high-frequency transformer [4]. This is designed to raise the voltage from the 12 V or 24 V of the accumulator to the 96 V load voltage. High current peaks and thermal management are important issues that should be considered. At the same time, the circuit size is reduced by using a 5 MHz switching frequency. A typical load power profile absorption is shown in Figure 2.

Considering the GaN devices for the switches in this circuit, only a worst case upper bound statistic can be found with 60 % confidence. Still, only with high temperature reverse bias, high temperature gate bias, high temperature and high relative humidity reverse bias, the failures have a relevant FIT rate of about 300 to 1600 FITs [5].

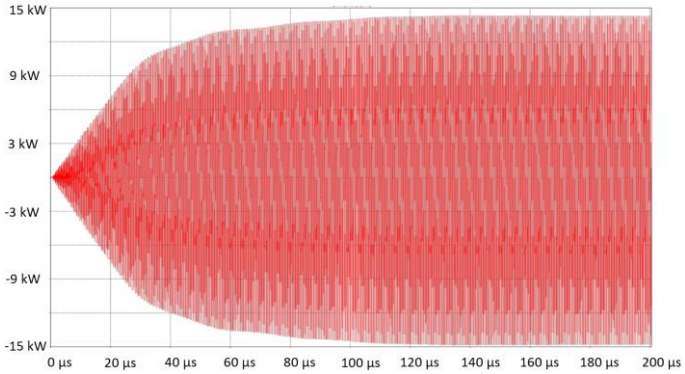

Figure 2. Typical load power profile absorption simulation.

2. High-frequency transformer challenges

High frequency effects like skin and proximity should be properly addressed [6]. Considering the 5 MHz switching frequency, proper core geometry and material are very difficult to be found. In this work, a coreless transformer is proposed to eliminate magnetic core limitations (in terms of thermal issues) and losses [7]. Nevertheless, eddy currents should be avoided, and an optimal magnetic coupling needs to be obtained.

Skin effects are an important issue for high frequency, high current applications, defining thin conductors rather than thick conductors. Capacitance coupling should be taken into consideration, as well. Energy transfer between stages without respecting the winding turns ratio of the transformer should be limited.

Thermal hot spots are a critical point for the insulation when peaks of current distribution are way higher than the average current, resulting in a high copper dissipation.

In this work, a 3D printed copper coreless transformer solution is investigated for a first prototype. Considering the required production rate in a high-volume manufacturing, final solution should consider a dedicated mold.

For the transformer a toroidal shape was chosen. In fact, that kind of geometry allows to obtain quite a good management of the induction field lines: in coreless transformers, in fact, it may be difficult to confine the field inside the device well and determine the real field lines pattern, usually not properly defined. As shown in the following paragraphs, leakage magnetic flux and, consequently, possible electromagnetic interferences (EMI) with nearby devices, are typical issues of coreless transformers, especially with high frequency and power rates: the toroidal shapes, unlike other kinds of geometries, such as the cylindric ones, should help to avoid that kind of problems, having quite a predictable magnetic field behavior, with a properly defined magnetic circuit.

3. Optimal transformer geometry definition

A first geometry of the transformer with adjacent designed windings is shown in Figure 3. The two windings have a turns ratio of 1:12, with 2 turns on the primary winding and 24 turns on the secondary one. This enables to boost from 12 V accumulator voltage to the 96 V desired on the load. However, this geometry has an important leakage flux, due to the lack of a core and the external distance between turns. Furthermore, the magnetic coupling between primary and secondary windings is not uniform, because of the non-distributed primary winding, completely separated from the secondary one.

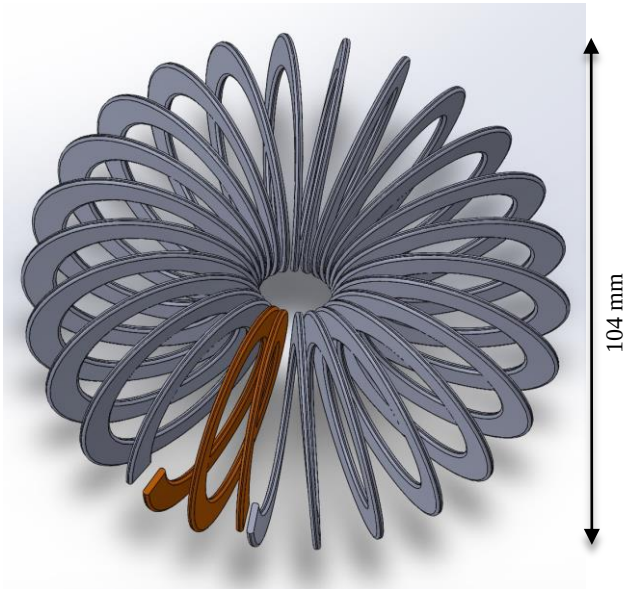

Figure 3. Contiguous windings designed transformer geometry (primary winding in brown).

A second and more optimized geometry with interleaved windings is shown in Figure 4. In this geometry, chosen for evaluating a method to obtain a good magnetic coupling, the turns ratio is 1:1 with a complete winding interleaving for a good evaluation of the magnetic coupling. The geometry, still good for galvanic insulations, was defined keeping as little space as possible to separate primary and secondary coils, which allows to concatenate the field close to themselves. In this case, the magnetic coupling shows satisfactory results and very low leakage flux is expected, with a very uniform induction magnetic field inside the device: in fact, the structure is almost symmetric on all space axes. However, capacitive coupling is an important issue to be considered.

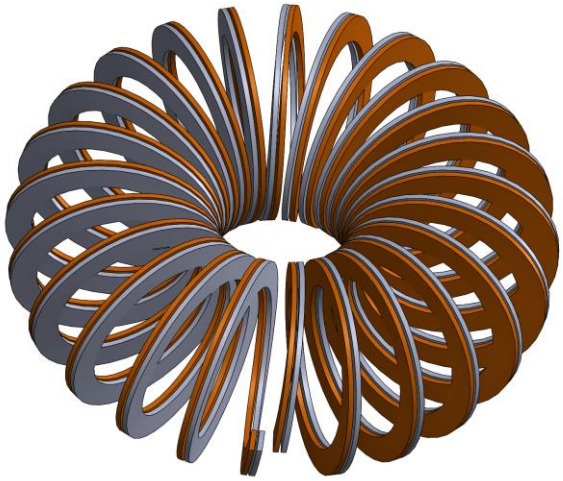

Figure 4. Interleaved windings 1:1 transformer geometry.

A third geometry with a 1:8 turns ratio and central connection adjustment was designed and shown in Figure 5.

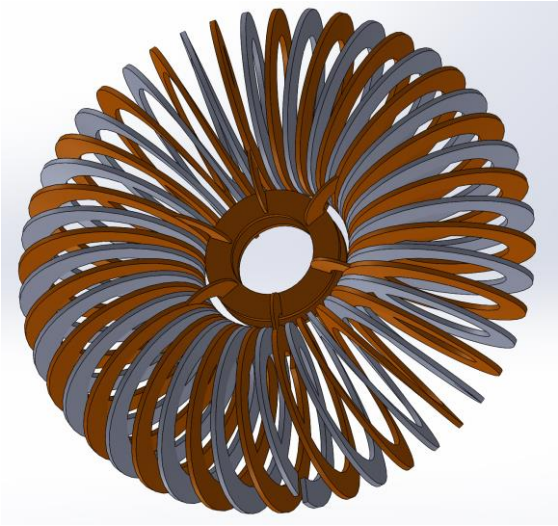

Figure 5. Central connection 1:8 turns ratio adjustment transformer geometry (primary winding in brown).

In this geometry, the primary and secondary windings are not interleaved as in Figure 4, and a lower magnetic coupling than the one of the interleaved with unitary turns ratio is expected. In this case, higher adjacent space between the windings and proper short circuits through an internal disk for obtaining the desired turns ratio are provided.

Finally, an interleaved geometry similar to the one shown in Figure 4 is proposed: the interleaved geometry, in fact shows a good magnetic coupling between windings. In this case, to obtain the desired transformer ratio the primary winding is reduced, occupying only a fraction of the circumference of the toroid, as shown in Figure 6. Also in this case, the primary not distributed causes a relevant leakage flux, but the results are more satisfying than the ones of the previous geometry.

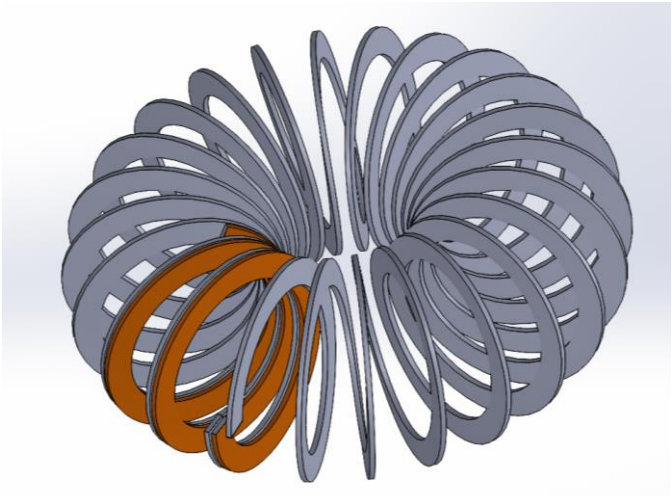

Figure 6. Interleaved structure with 1:8 turns ratio (primary winding in brown)

4. FEM simulation model

FEM simulations were carried out with COMSOL Multiphysics, analyzing both magnetic and electric (capacitive) effects. Thermal simulations were considered, as well. The Finite Element Analysis (FEA) procedure aims to show the magnetic field lines and to define the mutual inductance between the primary and the secondary windings, the coupling capacitance, and the impedance of the copper conductors [8]. Relevant consideration should be done on the mesh sizing. Skin effect, in particular, requires extremely small domains for accurate simulation results. Furthermore, a 0.1 m radius sphere has been designed to limit the 3D simulation space of the magnetic field. The induction magnetic fields magnitude on the surface of the sphere is almost negligible, so the radius length chosen is quite a good approximation. However, COMSOL allows to set infinite domains on the spheric surface: this could be a useful instrument to properly evaluate the correct behavior of the fields in the space. The materials set are the air of the sphere and the copper of the transformer windings. Each simulation is carried out with a resistive load of 2 Ω, reasonable load resistance; furthermore, some of them were carried out also with a load of 100 MΩ, considered a quasi-open circuit used for evaluating the mutual inductance.

For the electromagnetic analysis proper domain and boundary conditions were set: in particular, the induction magnetic field was computed thanks to Ampere's Law, applied to the windings. A magnetic insulation was applied to the spheric surface, as well. For simple electromagnetic simulations without thermal analysis, a 1 A sine wave current was set on the primary winding, with a frequency of 5 MHz.

Defining that kind of current, a magnetic flux density of approximately 10 μT to 0.5 mT can be observed around the transformer geometry.

Differently, thermal analysis can be carried out through stationary simulation, with proper boundary conditions: adequate natural air convection boundary conditions were applied to the simulation model, with an ambient temperature of 20 °C. Furthermore, a thin air layer was set between a couple of adjacent turns to simulate heat conduction without convection. Details of the model are shown in Figures 7 and 8. In this case, for the thermal analysis a 10 A amplitude current was set on the primary winding to obtain a more relevant result. Considering the dissipated active power on the copper windings overall temperature distribution can be extracted.

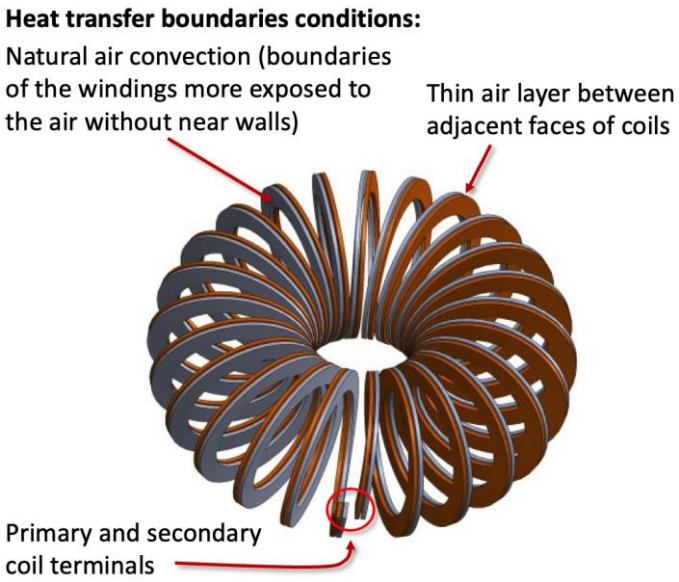

Figure 7. Electric and thermal model boundaries conditions

For each simulation a proper mesh was set, compatibly with the computational capabilities. In particular, in this structures, important proximity and skin effects are expected, and a proper mesh was set onto the boundary layers, in order to obtain a good current analysis.

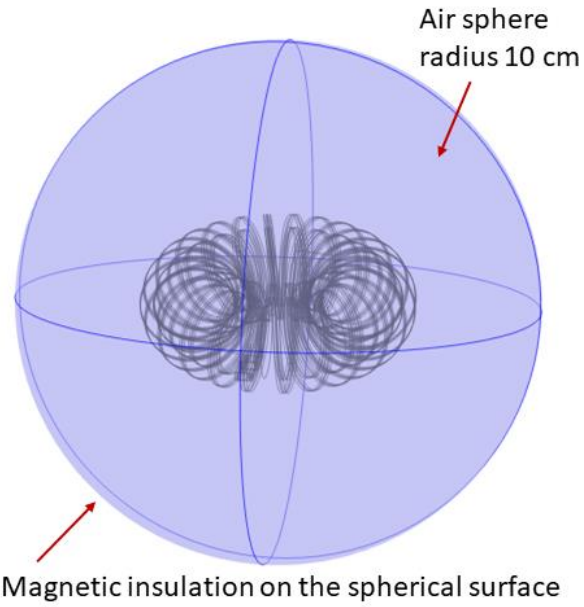

Figure 8. Other details of the model

A typical validation problem of FEMs is the consideration of the acceptable errors in the simulation results. Each simulation has been checked through numerical comparison, as for example the correspondence of the inlet and the outlet current of the windings. Then, current density, coil voltage, coil impedance, and temperatures are evaluated on both windings. Nevertheless, electrical measurements on a reference transformer have been carried out to validate the simulation results.

5. Simulation results

In this paragraph some of the most interesting results obtained are described. First, in Figure 9, qualitative magnetic fields lines for the interleaved 1:1 structure are shown: the magnetic coupling is very good, with very reduced leakage flux, and the calculated k factor is 96 %. Furthermore, magnetic flux was calculated on several points of the structure, showing a very uniform field in the toroid.

Proximity and skin effects are very relevant. In fact, these effects limit the current flow to few tens of μm below the surface of the windings (Figure 10). This thickness could be the copper boundary surface of windings fabricated with cheaper metals, such as aluminum. In this case, the calculation of the windings resistance with skin and proximity effects gave a reasonable value of about 0.5 Ω, similar to the one calculated analytically. This is the most promising and well-behaving between the analyzed geometries.

Analogous simulations were performed with the other structures shown in the previous images. In Figure 11 The central connection rings (see Figure 5) showed huge amounts of flux leakage. Further considerations are therefore not been analyzed in detail.

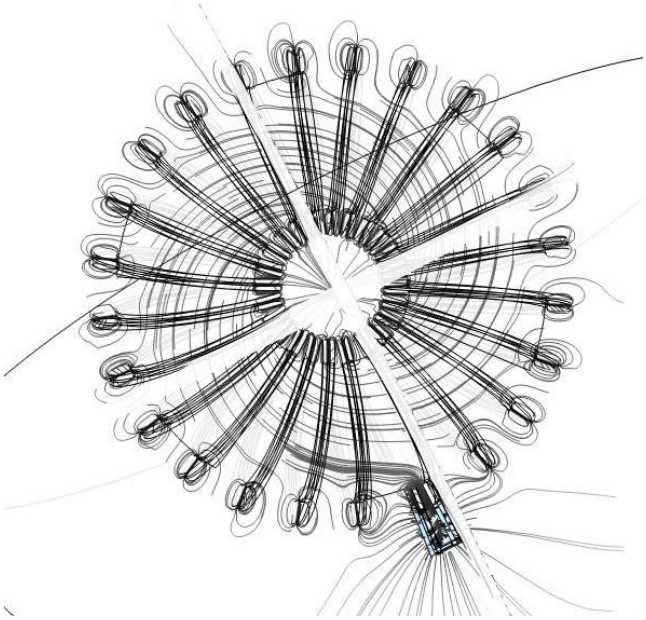

Figure 9. Magnetic induction field lines of the interleaved structure (top view), with 2 Ω real resistive load.

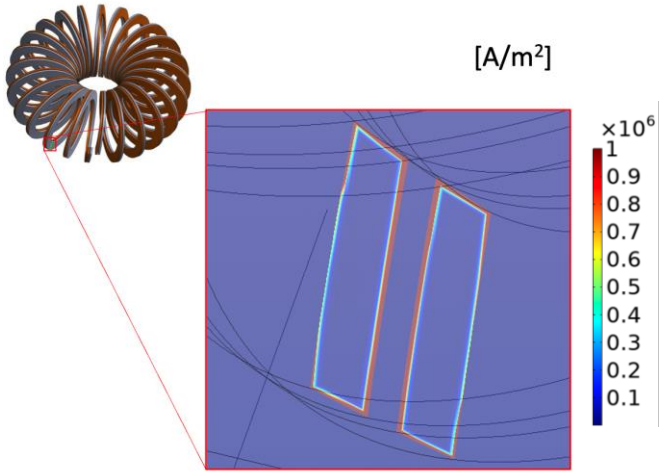

Figure 10. Current density norm graph in the 1:1 interleaved structure.

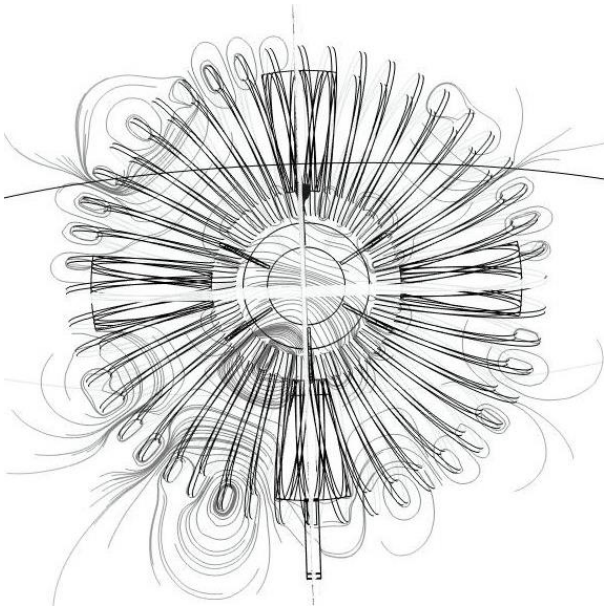

Figure 11. Magnetic induction field lines of the central connection ring interleaved structure (top view), with 2 Ω real resistive load.

The interleaved structure with non-unitary turns ratio, shown in Figure 6, reveals a low flux leakage (but higher than the one of the 1:1 device). Nevertheless, it is not enough to obtain a good transformer with acceptable efficiency. In this case, the mutual inductance calculation gave a value of about 0.36 μH, one magnitude order below the one of the 1:1 geometry. The ratio between the current on the primary winding and the secondary one with 2 Ω load gave a value of about 10.4. Therefore, the real current ratio is not exactly equal to the turns ratio, which must be slightly increased in order to obtain the desired voltage and currents on the secondary, because of the more relevant flux leakages. Finally, an electric field analysis showed a high and uniform electric field between the two windings, and almost null elsewhere, underlining the almost inductive correct and desired behavior of the structure.

Eventually, an electro-thermal simulation was set, in order to evaluate and show the possibilities and the limits of the used model. The boundary conditions are described in the previous section. In particular, as example, the interleaved structure with unitary turns ratio (see Figure 4) was simulated with a 10 A amplitude current on the primary winding. During the first study step a usual frequency-domain electromagnetic analysis (with a linearized model and large signals) was set, allowing an estimation of the active power losses (Joule effect and hysteresis) on the windings: that values were used in the second step, where a stationary thermal analysis was performed. The global simulation was computed with a segregated solver. In Figure 12 the thermal map on the windings is shown, with an ambient temperature of 20 °C. The thermal values obtained with a 10 A amplitude current are reasonable and not dangerous for excessive overheating, in spite of skin and proximity effects. Nearby the windings terminals an increase of temperature is observed, because of the local increase of resistance, which should be mitigated with a proper design of the connection terminals, in a possible future development of this work. Nevertheless, the temperature is quite uniform on the structure. As a future development of this research activity, a simulation with very high current could be set, also with a time domain thermal analysis.

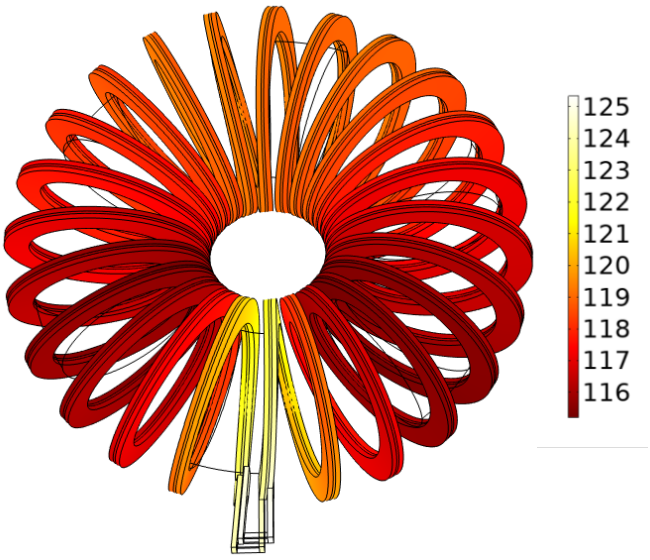

Figure 12. Thermal map on the windings surfaces. Colour bar in degrees Celsius.

6. Prototype and experimental results

6.1 Test introduction

The aim of this test is to prove coupling capability for this kind of solution. Coupling factor is equal to:

$$k = \frac{M}{\sqrt{L_{11}L_{22}}} \tag{3}$$

where $M = M_{12} = M_{21}$ is the mutual inductance and L_{11} and L_{22} are the self-inductances of primary and secondary windings, respectively. Transformer equations are the following:

$$\begin{cases} V_1 = (L + L_{l1})\dfrac{di_1}{dt} + M_{12}\dfrac{di_2}{dt} \\ V_2 = (L + L_{l2})\dfrac{di_2}{dt} + M_{21}\dfrac{di_1}{dt} \end{cases} \tag{4}$$

Self-inductance can be measured using an LCR meter plug on single winding, with the opposite side of the transformer open in order to have $M \cdot di/dt$ equal to zero.

Mutual inductance can be obtained by measuring the derivative of current over time when it crosses the zero (maximum value for sinewave) and measuring the maximum value of voltage at the secondary side.

The circuit shown in the schematic of Figure 13 is used to generate an AC current that flows on primary side winding, which can be measured using a current probe plug into an oscilloscope; at the same time, it is possible to measure the voltage induced on the secondary winding.

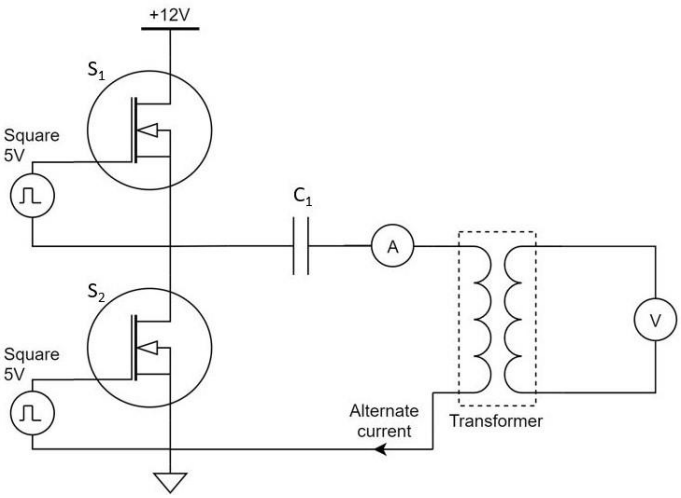

Figure 13. Schematic used for testing the transformer.

6.2 Test setup

A transformer prototype was realized using a 3D printed ABS toroid with helical grooves (Figure 14) to house Litz wires in order to test a similar solution as the model used for FEM analysis. Flat wires were replaced by Litz wires with features shown in Table 1.

Table 1. Litz wires features.

Strand Diameter	Number of strands	Section of conductors
30 μm	1000	0.7069 mm^2

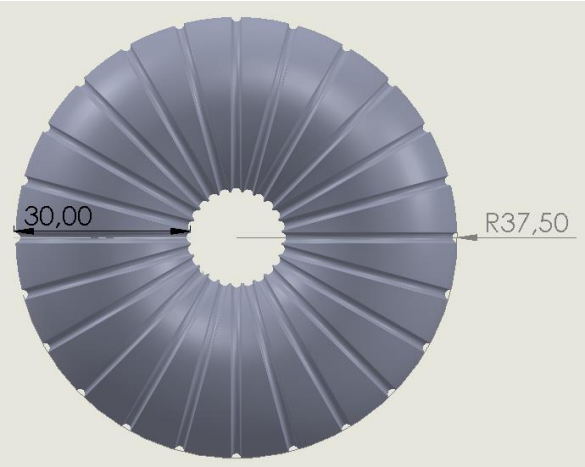

Figure 14. ABS toroidal support outlines. Dimensions are in mm.

The transformer is made to work at high frequency, so the driver was chosen considering a 5 MHz switching capability. A large amount of power is not needed, and it is a low voltage application.

A half bridge circuit drives the primary side of the transformer. GaN FETs are useful for this high frequency application. Then, a board from EPC was chosen (Figure 15). Decoupling capacitors were used to filter the current and obtain a sine wave with low distortion. MLC 0603 capacitors with NPO dielectric have the self-resonant frequency higher than current sine wave, so these devices were exploited for this application.

Figure 15. 60V 40A half bridge board (EPC9033), equipped with GaN devices.

Figure 16 shows the transformer plugged to the driver board. In particular, close to the letter A there are the filter capacitors, near B there are GaN FETs, and near C the primary side wire that is soldered on the board. The secondary side wiring is under the transformer.

6.3 Test results

The self-inductances of primary and secondary windings were measured using Keysight E4982A, obtaining the following values:

$$L_{11} = 4.72\ \mu H \quad (5)$$

$$L_{22} = 5.95\ \mu H \quad (6)$$

Figure 17 shows the oscilloscope screen capture during the measurement.

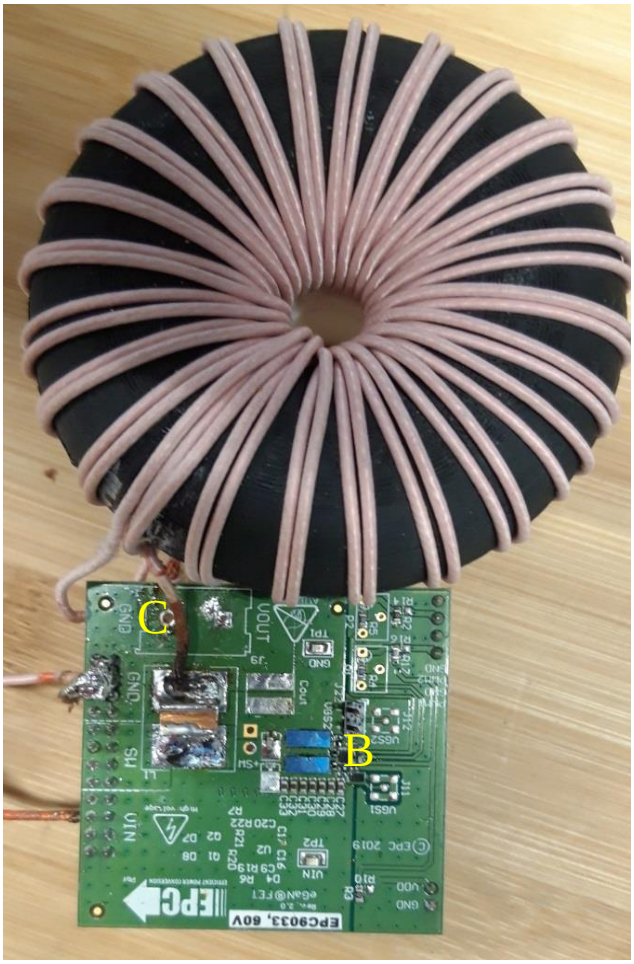

Figure 16. Device under test with driver. (A: filter capacitors; B: GaN FETs; C: primary winding wire).

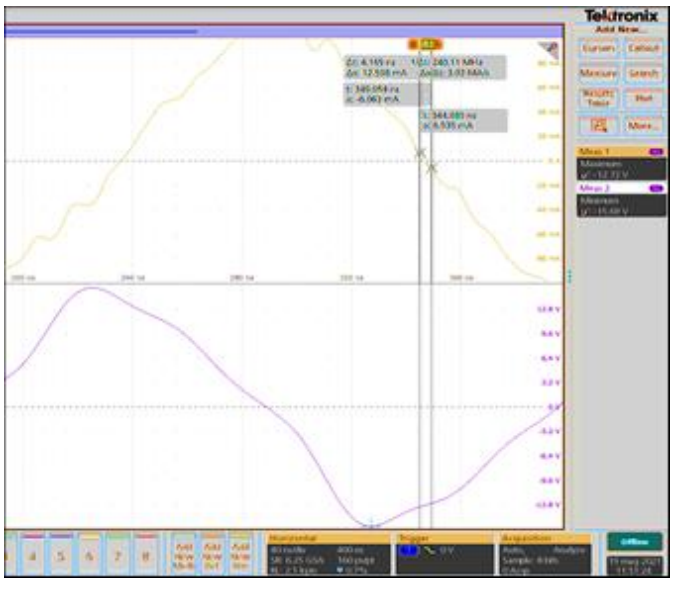

Figure 17. Scope capture showing voltage and current measured on the DUT.

The current derivative is

$$\frac{di_1}{dt} = 3.02\ \frac{A}{\mu s}, \tag{7}$$

while

$$V_{2,pk} = 15.69\ V, \tag{8}$$

the mutual inductance obtained is

$$M\ =\ 5.02\ \mu H, \tag{9}$$

and the coupling factor is

$$k\ = 0.98. \tag{10}$$

The current probe used during test has limited bandwidth, and the current measured includes several HF harmonics, so it is not possible to obtain a sine wave.

A parameter which can be compared between measurement and simulation results is the coupling factor k. The k factor of the 1:1 FEM simulation interleaved structure gave a value of 96 %, compared to 98 % (eq. 10) from the measurements on the test bench. Therefore, a very good matching can be seen between the simulation and the behaviour of a real device. Other comparisons between simulations and experimental, such as between the single inductances of the primary and the secondary windings, would be meaningless, due to the different types of conductors (i.e., different shape, section, etc.). In fact, simulations are based on conductors with rectangular section, differently from the one built for the measurement test bench, equipped with Litz wires.

These are preliminary results to verify the capability of this solution. In any case, as described in the previous paragraph, the coupling factor is similar to one obtained from simulation, and this confirms the usefulness of this solution for the power conversion for frequencies of several MHz.

7. Conclusions

High-frequency DC/DC converters for reliable boost circuits in automotive applications represent a very promising and cutting-edge solution. However, designing HF coreless transformers is not an easy task. The simulations described in the previous paragraphs show some critical aspects as well as interesting features and performances. First, the skin and proximity effects, as shown, make the current flow almost only on the surface of the conductors: this may lead to important overheating and electromigration issues. Another solution, that will be analyzed deeply in the final paper, is a transformer geometry equipped with Litz wires for the windings. This solution is less expensive than a 3D ad-hoc printed copper geometry, improving the reliability of the transformer, as well.

On the other hand, frequent high vibrations in the automotive applications and mechanical stresses could be critical, and proper simulations and tests must be carried out. These aspects could be interesting and useful for the future development of this work and will be discussed in the final paper. Moreover, electromagnetic and thermal FEM simulations, as shown in the previous paragraph, proved to be a very important and interesting instrument for the design of power devices. The use of numerical models based on FEM can be useful in the way forward to setup an optimization algorithm in order to identify the windings geometries able to improve the electro-magnetic and thermal features.

References

[1] S. G. Parler, E. P., et al., "Reliability of CDE Aluminum Electrolytic Capacitors", CDE Application Note, 2004.

[2] W.U. Xiaojuan, et al., "Reliability of high energy density ceramic capacitors", *Procedia Engineering*, vol. 45, pp. 998-1003, 2012.

[3] B. Abdi, et al., "Reliability Considerations for Parallel Performance of Semiconductor Switches in High-Power Switching Power Supplies", *IEEE Transactions on Industrial Electronics*, vol. 56, no. 6, pp. 2133 - 2139, 2009.

[4] Y. Du, S. Lukic, B. Jacobson and A. Huang, "Review of high power isolated bi-directional DC-DC converters for PHEV/EV DC charging infrastructure", 2011 IEEE Energy Conversion Congress and Exposition, 2011, pp. 553-560, doi: 10.1109/ECCE.2011.6063818.

[5] C. Jakubiec, "EPC eGaN FETs Reliability Testing: Phase 8", 2019.

[6] B. Abdi, "Winding Considerations on the High Frequency Transformers", *Energy Procedia*, vol. 12, pp. 656-661, 2011.

[7] K. Dawood, G. Komurgoz and F. Isik, "Modeling of Distribution Transformer for Analysis of Core Losses of Different Core Materials Using FEM", 2019 8th International Conference on Modeling Simulation and Applied Optimization (ICMSAO), 2019, pp. 1-5, doi: 10.1109/ICMSAO.2019.8880392.

[8] J. Cheng, P. Werelius and M. Ohlen, "FEM analysis of the transformer insulation XY model", PES T&D 2012, 2012, pp. 1-5, doi: 10.1109/TDC.2012.6281667.